On-Demand RIS-Assisted Free Space Optical Access System for 6G Networks

Alain R. Ndjiongue, *Senior Member, IEEE*, Octavia A. Dobre, *Fellow, IEEE*, and Hyundong Shin, *Fellow, IEEE*

***Abstract*—In reconfigurable intelligent surface (RIS)-assisted systems where the line-of-sight (LoS) path is entirely obstructed, there are the same number of RIS elements as pilot signals. This makes RIS implementation challenging and incurs signaling costs. In addition, there is power consumption due to multiplicative fading resulting from the fact that each RIS element induces two sub-channels. Therefore, a permanent use of the RIS module when not needed can be seen as resource mismanagement. A solution to reduce this cost and power consumption is the use of the RIS technology on-demand (OnD). This offers resource management, cost, and energy efficiency advantages. Reflecting on this situation, in this paper, we analyze a free space optical (FSO) system aided by the OnD RIS technology. We consider that the LoS link can be severely obstructed and its channel significantly degraded. This degradation affects the signal-to-noise ratio (SNR) of the LoS path, γ_o. We set its threshold value, γ_{th}, which corresponds to the system's triggering point. The analysis considers three main scenarios, namely $\gamma_o > \gamma_{th}$, $\gamma_o \leq \gamma_{th}$ with total interruption of the LoS link, and $\gamma_o \leq \gamma_{th}$ with gradual degradation of the LoS link. For these three scenarios, we define the sub-channel SNRs, derive the end-to-end (e2e) channel statistics, including the probability density functions, cumulative distribution functions, and moment-generating functions, for the LoS link alone, the non-LoS path through the RIS module alone, and the combined LoS and non-LoS paths. Furthermore, we derive, analyze, and evaluate the e2e ergodic channel capacity and average bit error rate, and provide results. We demonstrate that when the LoS link experiences high disturbances, a RIS module can restore the LoS system's performance for a specific time slot. Finally, we show that the RIS can be solicited in an OnD manner to prevent FSO degradation when the weather condition worsens.**

***Index Terms*—On-demand reconfigurable intelligent surfaces (OnD RIS), RIS-assisted free space optical (FSO) systems.**

I. Introduction

OPTICAL wireless communications such as visible light communication (VLC) and free space optical (FSO) communication are playing an increasingly significant role in the deployment of the next generation of mobile systems [1], [2], [3], [4], [5], [6], [7], [8], [9], [10]. VLC is remarkably useful indoors to assist with meeting the required transmission rate in environments hostile to the radio frequency (RF) signal or sensitive environments where the RF signal may cause major interference problems. On the other hand and due to its directional beams, the FSO technology is highly recommended for access systems. Its utilization becomes progressively imperative in the fifth generation (5G), beyond 5G (B5G), and sixth generation (6G) networks [6], [7], [8], [11]. Another reason for this is its ability to offer higher transmission rates and unregulated bandwidths. This higher transmission rate is needed in the deployment of B5G and 6G systems for multiple reasons. An example of 6G systems requiring FSO technology can be described as follows: Imagine a cloud radio access network (C-RAN), where the base stations contain radio units, central processing units, and broadband processing units that need to be interconnected [12], [13]. Due to the amount of data transmitted between these units and C-RAN, a high data transmission link is necessary. FSO is seen as one of the most suitable technologies to connect these units, given that it will offer the required high data transmission link without creating inter-channel interference between the links.

FSO systems are characterized by the absence of non-line-of-sight (NLoS) links between transmitters and receivers [14]. This exposes FSO systems to signal loss if the LoS path is obstructed and represents a major problem for the access system given that users are not willing to accept service disruptions or link disconnections when browsing on their terminals. An efficient solution to this dilemma is the implementation of reconfigurable intelligent surfaces (RISs), which allows the system to meet the performance obtained under normal circumstances, i.e., when the LoS link is not disrupted [11], [14], [15], [16]. Taking the above example, i.e., C-RAN, its associated units, and the RIS technology, the cost of implementation and operation may be higher for the next generation of mobile systems, including 6G. Solutions that can minimize this cost and power consumption are welcome. To this end, we propose in this paper the analysis of an on-demand (OnD) RIS-assisted FSO access system for 6G networks.

Several sources of impairment may affect the LoS signal in FSO systems. They include newly constructed buildings, clouds, rain, fog, and adverse weather. When compared to newly constructed buildings, degradation due to cloud, rain, fog, and other weather conditions is not permanent. For example, clouds move, and even if their speed is noticeably low, they will free up

Received 21 April 2024; revised 24 October 2024; accepted 15 January 2025. Date of publication 23 January 2025; date of current version 20 June 2025. This work was supported in part by the Natural Sciences and Engineering Research Council of Canada (NSERC), through its Discovery program. The review of this article was coordinated by Dr. Sinan Gezici. *(Corresponding authors: Octavia A. Dobre; Hyundong Shin.)*

Alain R. Ndjiongue is with the School of Electrical and Information Engineering, Faculty of Engineering and the Built Environment, University of the Witwatersrand, Johannesburg 2050, South Africa.

Octavia A. Dobre is with the Faculty of Engineering and Applied Science, Memorial University, St. John's, NL A1C 5S7, Canada, and also with the Department of Electronic Engineering, Kyung Hee University, Yongin 17104, South Korea (e-mail: odobre@mun.ca).

Hyundong Shin is with the Department of Electronics and Information Convergence Engineering, Kyung Hee University, Yongin-si 17104, South Korea (e-mail: hshin@khu.ac.kr).

Digital Object Identifier 10.1109/TVT.2025.3532988

the transmission environment. Their speed depends on a variety of factors, including cloud type, wind speed, and direction. It is reported that the average cloud moves at a speed lower than 10 km per hour. This implies that, depending on the cloud size, the LoS link can be interrupted for an hour or more. Also, adverse weather conditions can last from an hour to days, weeks, or months. During this time, the LoS link can be totally disrupted or degraded, and therefore, needs assistance. However, when the obstacle disappears, this assistance is no longer required. The RIS technology can be efficiently used to restore the LoS conditions of the FSO system during degradation. The use of the RIS technology as a permanent solution to this type of LoS FSO link blockage may be considered resource misuse. The RIS module may induce cost and consume energy. It is well-known that signaling overhead is required for channel estimation and beamforming in real-time. Nevertheless, in a RIS-assisted FSO system, the number of pilot signals equals the number of RIS elements. This results in high overhead signaling that will make the application of RIS with a large number of passive elements significantly challenging due to multiplicative fading caused by the RIS module [17]. This high overhead signaling incurs cost [18], while multiplicative fading, which is solved using RIS with active elements [11], [19], induces power consumption. Consequently, it will be beneficial to disconnect the RIS module when the obstacle on the LoS link disappears, leading to the use of the OnD RIS technology. In addition to the above motivation, a number of scenarios favor the use of the RIS technology in an OnD manner. For instance, (i) the RIS module can be attached to a drone, an unmanned aerial vehicle, or to equipment on high-altitude platforms; (ii) The environment to be reinforced is infrequently used, and the RIS module may be unnecessarily connected for a long time; (iii) In many situations, the RIS module is required to improve transmission when the LoS link is weak or not available due to channel conditions or obstacles. When the LoS link becomes available to ensure that the targeted service level is met, the RIS module can be turned off.

A plethora of research outputs can be found in the literature on RIS-assisted FSO systems [6], [7], [11], [14], [20], [21], [22], [23], [24], [25]. Below, we provide a quick overview of these works. In [14], the authors tackle the skip zone dilemma in the FSO environment using the RIS technology. They consider turbulence and pointing errors in a near-terrestrial environment following the Gamma-Gamma (GG) distribution. The authors of [20] evaluate the system and channel models and present the RIS-based FSO system geometry. They propose conditional geometric and misalignment losses (GML) vs. misalignment for different RIS sizes. This work shows how to derive the probability density function (PDF) of the GML for the RIS-based FSO link. As in [14], [20] also considers the GG distribution with several levels of turbulence and pointing errors. In [22], the authors exploit the Huygens-Fresnel principle to forge an analytical end-to-end (e2e) channel model for RIS-assisted FSO systems. The results show the pointing displacement in terms of the lens xy coordinates. The paper also provides the average bit-error rate (BER) versus the RIS-receiver distance and geometric far-field approximation. In [21], [23], [24], [25], the authors deal with an RIS-based FSO system using an unmanned aerial vehicle (UAV). An intelligent reflecting surface carried by an unmanned aerial vehicle is proposed by the authors of [21] to provide laser path controllable FSO communication. To quantify the physical impacts of the system, generalized atmospheric turbulence, modeled as the GG distribution, has been used, and the Hoyt distribution has been used to model specified pointing error loss. A secure transmission design for a RIS-assisted UAV network is explored in [23] in the presence of an eavesdropper. A combined optimization of the UAV trajectory, the transmitted beamforming, and the phase shift of the RIS is used to maximize the average secrecy rate. The authors of [24] use the RIS technology to enhance the performance of UAV-assisted air-ground networks. They also present an overview of the combination of UAV and RIS by introducing a variety of applications for RIS as well as the attractive advantages of UAV and highlighting the advantages of combining the two technologies. [25] presents a scheme for integrating RIS and UAV communication, in which the RIS is mounted on the UAV to provide a connection between the base station and the ground station. Two schemes have been developed to maximize the spectrum efficiency and the energy efficiency of the system by optimizing active beamforming, passive beamforming, and UAV trajectory simultaneously. Some studies focus on the practical implementation of RIS-based FSO systems. For example, in [6], the authors investigate the suitability of FSO links for 6G applications using a field-programmable gate array. They study how to develop a prototype, considering various transmission scenarios over the FSO channel. In this work, the authors employ the Mach-Zehnder modulator to model the two-dimensional atmospheric channel. The above works show that research on RIS-aided systems is advancing rapidly, and prototyping and mass production will follow. Another example of works related to prototyping is provided in [7], where the authors propose the concept of modular FSO transceivers to facilitate modules' customization. In most of these works, the RIS technology is introduced to solve dead zones in the system or recover the LoS system performance when the LoS link is obstructed. Another reason for studying RIS-assisted systems is to reinforce the NLoS link to ameliorate the signal-to-noise ratio (SNR), enhance spectral efficiency and receive signal power [11], [25].

The above brief review shows that the RIS technology is generally used in FSO to create an NLoS link that can mimic the LoS system's performance. It also shows that the use of the RIS module is not permanently required in some cases. It can therefore be used in an OnD manner in those cases. To the best of the authors' knowledge, an analysis of FSO systems assisted by the RIS technology where the RIS module is enabled for a specific time slot has not been presented in the open literature, even in [26], where the concept of OnD RIS was coined for the first time. This represents an open research gap. In this paper, we fill up the gap and provide an analysis of an OnD RIS-assisted FSO system. To this end, we summarize our contributions as follows:

- We consider FSO systems modeled using the GG distribution, where a temporary obstacle may cause the LoS link

to lose connection or its channel to degrade for a short period. We analyze the OnD RIS technology to assist this transmission, solve the effects of temporary obstacles, and mimic the LoS performance obtained when the LoS link is not obstructed or does not degrade. Such an environment is affected by a cloud, wind, rain, and any other types of obstacles or impairment sources that can temporarily impede the LoS path.

- We study the proposed OnD RIS-assisted FSO system considering three main scenarios: (i) The LoS link alone; (ii) The NLoS path through the OnD RIS module alone; (iii) Both links combined using the maximum ratio combining (MRC) technique. For these three scenarios, we study the e2e channel SNR and derive the corresponding statistics, including the PDF, cumulative distribution function (CDF), and moment-generating function (MGF). Afterward, we obtain the corresponding e2e performance metrics, namely the ergodic channel capacity, $\overline{C}_{e2e}$, and the average BER, $\overline{P}_{e2e}$. To evaluate the average BER, we consider the coherent binary phase shift keying (CBPSK) modulation scheme, taken as an example.
- We assess the ergodic channel capacity and average BER concerning average e2e SNR, taking into account multiple turbulence effects and pointing errors to show the switching episodes between the considered scenarios (LoS, NLoS, and combined LoS and NLoS links).
- Finally, we discuss how to optimize the system to show that the OnD RIS can be used to anticipate LoS link degradation by setting a higher threshold value to the e2e SNR.

A. Notation and Theorems

Selected notations are presented in Table I. In the sequel, the term "unified" means including both turbulence and pointing error parameters in one expression. Below are the theorems, concepts, and relationships used in the paper.

Theorem 1: The PDF, $f_{Y_1,Y_2,\ldots,Y_N}(y_1, y_2, \ldots, y_N)$, of N jointly continuous and independent random variables y_1, y_2,..., y_N can be expressed as a multiplicative condition as [27]

$$f_{Y_1,Y_2,\ldots,Y_N}(y_1, y_2, \ldots, y_N) = \prod_{n=1}^{N} f_{Y_n}(y_n). \tag{1}$$

Theorem 2: Let x be a continuous random variable with PDF $f_X(x)$ and g: $\mathbb{R} \Longrightarrow \mathbb{R}$, a strictly continuous monotonic differentiable function such that $Y = g(X)$. The PDF of Y can be given by [28]

$$f_Y(y) = f_X\left(g^{-1}(y)\right)\left|\frac{\partial g^{-1}(y)}{dy}\right|. \tag{2}$$

Theorem 3: The CDF, $F_Y(y)$, of a random variable y can be evaluated as $F_Y(y) = \int_0^\infty f_Y(y)dy$ [14]. A change of variable of the type

$$F_Y(y) = \int_0^y f_Y(t)dt, \tag{3}$$

can be used, and the integral can be readily solved with the help of [29, Eq. (07.34.21.0084.01)].

TABLE I
SELECTED NOTATION

Symbol	Definition
S-D	Source-destination path (LoS)
S-RIS-D	Source-RIS-destination path (NLoS)
α, β	Turbulence parameters
ξ	Pointing displacement coefficient
o	Index of the LoS link
d	Index of the NLoS link
c	Index of the combined S-D and S-RIS-D links
h	Index of the S-RIS link
g	Index of the RIS-D link
mrc	Superscript related to maximum ratio combining technique
$e2e$	Index representing the e2e system considering S-D and/or S-RIS-D paths
Δ	Index related to optimized parameters
γ	Signal-to-noise ratio
$f_Y(y)$	Probability density function of y
$F_Y(y)$	Cumulative distribution function of y
$\Omega_y(s)$	Moment generating function of y
$\overline{C}$	Ergodic channel capacity
$\overline{P}$	Average BER

$\mathbb{E}[\cdot]$ denotes the expectation operation and $p_r(\cdot)$ represents the probability operator.

Theorem 4: The MGF, $\Omega_X(s)$, of a random variable x can be evaluated as $\Omega_X(s) = \mathbb{E}[e^{-xs}]$. This expression can be represented in integral form as [14], [30]

$$\Omega_X(s) = s\int_0^\infty \exp[-xs]F_X(x)dx. \tag{4}$$

The integral in this equation is readily solved with the help of [31, Eq. (7.813.1)].

Theorem 5: The ergodic channel capacity, $\overline{C}_i$, of a transmission system can be evaluated using the PDF of the transmission SNR as $\overline{C}_i = [W/\log(2)]\int_0^\infty \log[1 + e\gamma_i/(2\pi)]f_{\gamma_i}(\gamma_i)d\gamma_i$. By exploiting the Meijer-G expression of $\log[1 + e\gamma_o/(2\pi)]$ [29, Eq. (07.34.03.0456.01)], this expression can be reformulated as [32]

$$\overline{C}_i = \frac{W}{\log(2)}\int_0^\infty \mathbf{G}_{2,2}^{1,2}\left[\frac{e\gamma_i}{2\pi}\middle|\begin{matrix}1,1\\1,0\end{matrix}\right] f_{\gamma_i}(\gamma_i)d\gamma_i, \tag{5}$$

and the integral can be solved with the help of [29, Eq. (07.34.21.0013.01)].

Theorem 6: The average BER of a communication system using binary schemes can be evaluated using [32, Eq. (13)]

$$\overline{P}_i = \frac{b^a}{2\Gamma(a)}\int_0^\infty e^{-b\gamma}\gamma^{a-1}F_{\gamma_i}(\gamma_i)d\gamma_i, \tag{6}$$

where the pair (a, b) denotes the binary modulation schemes [30]. The values of a and b for selected modulation schemes, namely coherent binary frequency shift keying, non-coherent binary frequency-shift keying, CBPSK, and differential phase shift keying, are respectively given by the pairs (0.5, 0.5), (1, 0.5), (0.5, 1), and (1, 1) [32].

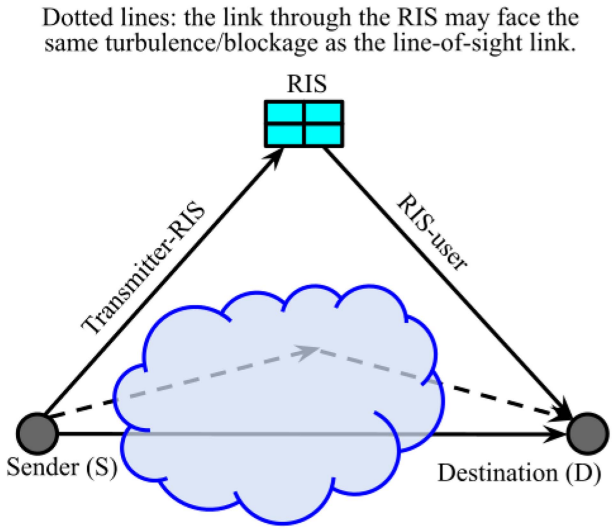

Fig. 1. A generalized model of OnD RIS-assisted FSO systems.

II. System and Channel Description

A. System Model

Consider the FSO link between two city buildings, where S and D are situated at a known distance from each other, as depicted in Fig. 1. Three main factors affect data transmission in this type of FSO environment. These include attenuation, pointing errors, and turbulence. Attenuation is generally given by the Beer-Lambert law. In this analysis, it is considered constant for a given weather condition and link distance [30]. Turbulence is characterized by its α-β parameters and the pointing error by the pointing displacement, ξ.

Due to bad weather, the LoS link between the two buildings is interrupted. During the interruption time, an RIS module is activated and inserted into the transmission system to ensure the continuation of data transfer between the sender and destination. The RIS module is located over a third building at specific distances from S and D. The sender generates many light rays, which are all reflected by the RIS module, made of M elements, toward a single receiver. To ensure that all reflected light rays are smoothly directed to the unique receiver, the RIS elements have variable refractive indices. This provides the advantage of electrically controlling light passing through the RIS module, without a micromechanism. The receiver is made of a single photodetector. The overall environment follows the GG distribution and is governed by the same pointing error expression. However, the characteristics and parameters of the S-D and S-RIS-D links differ. The S-D link is subject to signal outages, while the S-RIS-D link is not.

B. Channel Model

We assume that the noise at D is additive, and its components are independent and identically distributed, and defined by $\mathbf{n} \sim \mathcal{CN}(0, \mathbf{I})$. The signal, $\mathbf{y}$, observed at D can be given by $\mathbf{y} = \mathbf{H}_{e2e}\mathbf{x} + \mathbf{n}$, where $\mathbf{x}$ is the data symbol at S [33], [34]. The matrix $\mathbf{H}_{e2e}$ may contain the transmit SNR and the active beamforming vector [34]. It is characterized by the state of the link between S and D, which is subject to attenuation, pointing errors, and turbulence. Depending of the state of the S-D link, $\mathbf{H}_{e2e}$ can bear three different expressions.

$$\mathbf{H}_{e2e} = \begin{cases} \mathbf{H}_o \ \text{ for LoS link alone, } (a) \\ \mathbf{H}_d = \mathbf{H}_h \Phi \mathbf{H}_g \ \text{ for OnD RIS alone, } (b) \\ \mathbf{H}_c \ \text{ for combined S} - \text{D and S} - \text{RIS} - \text{D.} (c) \end{cases} \tag{7}$$

The matrix in (7)–(a), $\mathbf{H}_o$, is a single-input single-output channel matrix between S and D in the scenario where the S-D SNR, γ_o, is greater than γ_{th}, while in (7)–(b) and (7)–(c), $\mathbf{H}_d$ and $\mathbf{H}_c$ relate to the scenarios where $\gamma_o \leq \gamma_{th}$ with total interruption of the S-D link and $\gamma_o \leq \gamma_{th}$ with slow degradation of the S-D link. $\mathbf{H}_h \Phi \mathbf{H}_g$ is defined in the $\mathbb{R}_+^{M \times M}$ space and its entries are the channel gains between the transmitter and receiver through the M OnD RIS elements. The corresponding phase shift matrix, Φ, is diagonal and defined in the $\mathbb{R}_+^M$ space, and given by $\Phi = \mathbf{diag}(\phi_1, \phi_2, ..., \phi_M)$, where $\phi_m = \lambda_m e^{j\alpha_m}$, with $\alpha_m \in [-\pi, \pi]$ [33], [34]. Note that $\lambda_m \in]0, 1]$ for conventional OnD RIS modules and $\lambda_m > 1$ for amplifying OnD RIS modules. The entries H_h and H_g of the components $\mathbf{H}_h$ and $\mathbf{H}_g$ are channel gains, respectively $\mathbb{R}_+^{1 \times M}$ for the S-RIS link and $\mathbb{R}_+^{M \times 1}$ for the RIS-D link, which, as the S-D link, follow the GG distribution.

In the sequel, we consider single S-D and S-RIS-D beams. Since heterodyne detection offers better performance than intensity modulation and direct detection, we consider a system in which the transmitted light intensity is modulated and heterodyne detection is employed. Let I_a, I_p, and I_t be the received intensities affected by attenuation, pointing error, and turbulence, respectively. The received intensity can be expressed as $I = I_a I_p I_t$ [30]. As attenuation is constant for a given weather condition and link distance, it is assumed that it does not influence the link SNR PDF. The PDF of the pointing error can be expressed as [14], [30]

$$f_{p,i}(I_{p,i}) = \frac{\xi_i^2}{A_{o,i}^{\xi_i^2}} I_{p,i}^{\xi_i^2 - 1}, \quad 0 \leq I_{p,i} \leq A_{o,i}, \tag{8}$$

where $i \in \{\text{S-D, S-RIS, RIS-D}\}$. ξ_i denotes the ratio of the equivalent beam radius to the pointing displacement standard deviation at the RIS and D, with $A_{o,i} = [\text{erf}(v_i)]^2$, where erf() is the error function at RIS and D, and $v_i = d_i\sqrt{\pi}/\sqrt{2}W_{z,i}$. $W_{z,i}$ and d_i are the beam waist and the radius of the receiver aperture, respectively. ξ_i is generally expressed as [14]

$$\xi_i = \frac{W_{eq,i}}{2\rho_i}, \tag{9}$$

where ρ_i is the jitter variance at the RIS and D, and $W_{eq,i}$ is given by [14]

$$W_{eq,i} = \frac{W_{z,i}\sqrt{\pi}\text{erf}(v_i)}{2v_i e^{-v_i^2}}, \tag{10}$$

with $W_{z,i}$ as the beam waist at the RIS and D, and d_i representing the aperture at the RIS and D. The atmospheric turbulence, which follows the GG distribution in the proposed system, is mainly characterized by strong and moderate turbulence levels. Its PDF

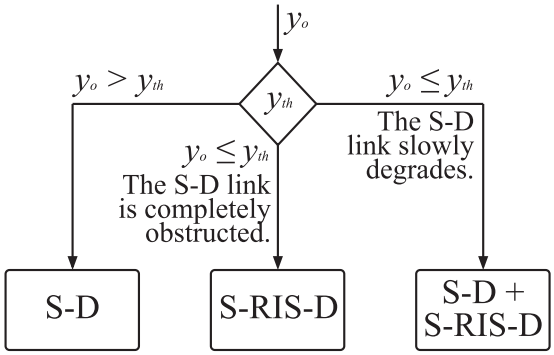

Fig. 2. Scenarios of OnD RIS commissioning in OnD RIS-assisted FSO systems.

can be given by [14]

$$f_{I_{a,i}}(I_{a,i}) = \frac{2(\alpha_i\beta_i)^{\frac{\alpha_i+\beta_i}{2}}}{\Gamma(\alpha_i)\Gamma(\beta_i)} I_{a.i}^{\frac{\alpha_i+\beta_i}{2}-1} \mathbf{K}_{\alpha_i-\beta_i}\left(2\sqrt{\alpha_i\beta_i I_{a,i}}\right), \tag{11}$$

where $\mathbf{K}_j$ denotes a second kind modified Bessel function of order j. In practice, the values of α_i and β_i are based on the Ritov variance given by $\sigma_i^2 = 0.492C_i^2\eta^{7/6}L^{11/6}$. C_i^2 is the altitude-dependent index that characterizes the transmission environment. $\eta = 2\pi/\lambda$ is the angular wave number, while L_i, α_i, and β_i are defined in [30].

III. Statistical Analysis

As shown in Fig. 2, the three scenarios analyzed are (i) $\gamma_{th} < \gamma_o$ (S-D link alone); (ii) $\gamma_o \leq \gamma_{th}$ (S-RIS-D link alone); and (iii) $\gamma_o \leq \gamma_{th}$ (S-D and S-RIS-D links combined). These are used to develop the OnD RIS commissioning algorithm (see Algorithm 1), which provides conditions and steps to enable the OnD RIS module.

The outage probability can be defined as the likelihood that a certain transmission rate will not be sustained due to channel variations. In an optical wireless channel, this definition can be materialized by the analysis of its ergodic channel capacity $\overline{C}_i$. The probability that the transmission rate goes below the threshold value, R_i, can be defined by $p_r(\overline{C}_i < R_i)$, where $p_r()$ is the probability operator. In our case, if the LoS link fails, the OnD RIS module is connected to create an NLoS link that ensures service continuity. The RIS activation is based on Algorithm 1, and considers the three main scenarios enumerated above. For a better understanding of such a system, we successively provide statistical and performance analyses for each scenario separately.

A. Sub-Channels' SNR

1) $\gamma_{th} < \gamma_o$, S-D Link Alone (LoS): In this scenario, the RIS module is in hibernation. Its elements do not participate in the communication operation. The message is carried through to the user via the S-D link. The e2e SNR is defined by $\gamma_o = \overline{\gamma}_o h_o^2 = E_{b,o}h_o^2/N_{0,o}$, with $\overline{\gamma}_o$ as the average SNR given by $E_{b,o}/N_{0,o}$, where h_o is the channel gain, $E_{b,o}$ denotes the bit energy, and $N_{0,o}$ stands for the PSD of the noise at D.

2) $\gamma_o \leq \gamma_{th}$, S-RIS-D Link Alone (NLoS): In this scenario, the S-D link is obstructed. The transmitted signal transits through the RIS module to reach the receiver. The e2e SNR can be defined as $\gamma_d = \overline{\gamma}_d(H_h\lambda_m e^{j\alpha_m}H_g)^2$, where H_h and H_g are the channel fading coefficient over the S-RIS and RIS-D links, respectively, while $E_{s,d}$ is the bit energy considering the S-RIS-D path, and $\overline{\gamma}_d = E_{s,d}/N_{0,d}$ is the corresponding e2e average SNR.

3) $\gamma_o \leq \gamma_{th}$, S-D and S-RIS-D Links Combined Using the MRC Technique: The scenario where $\gamma_o \leq \gamma_{th}$ with continuous degradation of the S-D link considers both the S-D and S-RIS-D links. This corresponds to the situation where the S-D link is considerably affected, but not completely obstructed. A combining technique is used to recover the transmitted bit. In this scenario, we discuss only the MRC technique because it is sufficient to describe the situation. Considering that the SNRs γ_o and γ_d over S-D and S-RIS-D links, respectively, are independent, Theorem 1 applies. The combined SNR, γ_c, can be given by [38, Eq. (4)]

$$\gamma_c = \frac{1}{\sqrt{L^{1-p+q}}}\left(\frac{E_s}{N_0}\right)\left[\sum_{l=1}^{L}\gamma_l^p\right]^q, \tag{12}$$

where E_s/N_0 is the transmitted SNR per symbol and $(p, q) = (2, 1)$ for MRC [38, Eq. (5)], with $L = M + 1$. For a normalized transmitted SNR per symbol in an MRC combination, $E_s/N_0 = 1$ [38], the combined SNR, γ^{mrc}, can be expressed as

$$\gamma^{mrc} = \gamma_o^2 + \gamma_d^2. \tag{13}$$

B. Sub-Channels' Statistics

1) $\gamma_{th} < \gamma_o$, S-D Link Alone (LoS): When the SNR of the S-D link, γ_o, is above the threshold value, its unified PDF, $f_{\gamma_o}(\gamma_o)$,

Algorithm 1: OnD RIS Commissioning Algorithm.

Input: γ_{th}, pilot signals, $E_{b,o}$, and ∂;
Evaluation: Channel estimation algorithms, [35]–[37];
Evaluation: $N_{0,o}$;
Evaluation: $\gamma_o = \overline{\gamma}_o h_o^2 = E_{b,o}h_o^2/N_{0,o}$;
Evaluation: $\gamma_d = \overline{\gamma}_d\left(H_h\lambda_m e^{j\alpha_m}H_g\right)^2$;
Evaluation: $\gamma_c = \frac{1}{\sqrt{L^{1-p+q}}}\left(\frac{E_s}{N_0}\right)\left[\sum_{l=1}^{L}\gamma_l^p\right]^q$;
Comparison:
if $\gamma_o \leq \gamma_{th}$, **then**
  do: RIS = 1.
  if $0 < \gamma_o \leq \gamma_{th}$, **then**
    do: $\gamma_{eq} = \gamma_o//\gamma_{ris}$
  end
  else
    do: $\gamma_{eq} = \gamma_{ris}$.
  end
end
else
  do: RIS = 0.
end

can be formulated using the Meijer-G function as [14], [30]

$$f_{\gamma_o}(\gamma_o) = \frac{\phi_o}{\gamma_o}\mathbf{G}_{1,3}^{3,0}\left[\frac{\psi_o\gamma_o}{\overline{\gamma}_o}\middle|\begin{matrix}\xi_o^2+1\\ \xi_o^2,\alpha_o,\beta_o\end{matrix}\right], \tag{14}$$

where $\phi_o = \xi_o^2/(\Gamma[\alpha_o]\Gamma[\beta_o])$, $\psi_o = \xi_o^2\alpha_o\beta_o/(\xi_o^2+1)$ [14], [30], and $\mathbf{G}_{p,q}^{m,n}\left[z\middle|\begin{matrix}a_p\\ b_q\end{matrix}\right]$ is the Meijer-G function [39]. We respectively apply Theorems 3 and 4 to (14). With a few mathematical operations, and respectively exploiting [29, Eq. (07.34.21.0084.01)] and [31, Eq. (7.813.1)], we obtain the corresponding unified CDF, $F_{\gamma_o}(\gamma_o)$, and MGF, Ω_{γ_o}, as

$$F_{\gamma_o}(\gamma_o) = \phi_o\mathbf{G}_{2,4}^{3,1}\left[\frac{\psi_o\gamma_o}{\overline{\gamma}_o}\middle|\begin{matrix}1,\xi_o^2+1\\ \xi_o^2,\alpha_o,\beta_o,0\end{matrix}\right], \tag{15}$$

and

$$\Omega_{\gamma_o}(s) = \phi_o\mathbf{G}_{3,4}^{3,2}\left[\frac{\psi_o}{s\overline{\gamma}_o}\middle|\begin{matrix}0,1,\xi_o^2+1\\ \xi_o^2,\alpha_o,\beta_o,0\end{matrix}\right]. \tag{16}$$

Note that the CDF and MGF in (15) and (16) correspond to those of an FSO link found in the literature, [30] for example. In the sequel, the proposed expressions of PDF, CDF, and MGF are unified.

2) $\gamma_o \leq \gamma_{th}$, S-RIS-D Link Alone (NLoS): In this scenario, the e2e channel is a concatenation of two parts, denoted by the indexes h and g, respectively, for the S-RIS and RIS-D link (of the S-RIS-D path). Three sections are involved in this transmission path, namely the S-RIS link, the RIS-D link, and the OnD RIS module. The RIS parameters are deterministic and independent of the transmission environment. Therefore, the SNR's PDF, which is that of a multiplicative convolution of the S-RIS and RIS-D sub-channels, considers the S-RIS and RIS-D sections. In the sequel, it is assumed that the PDFs $f_{\gamma_h}(\gamma_h)$ and $f_{\gamma_g}(\gamma_g)$ of these respective sub-channels reside in the same space. Their multiplicative convolution, $f_{\gamma_d}(\gamma_d)$, is readily evaluated by the product of their Mellin transforms as

$$f_{\gamma_d}(\gamma_d) = \tilde{f}_{\gamma_h}(\gamma_h)\tilde{f}_{\gamma_g}(\gamma_g), \tag{17}$$

where $\tilde{f}_{\gamma_h}(\gamma_h)$ and $\tilde{f}_{\gamma_g}(\gamma_g)$ are the Mellin's transforms of the PDFs $f_{\gamma_h}(\gamma_h)$ and $f_{\gamma_g}(\gamma_g)$, respectively. The product $\tilde{f}_{\gamma_h}(\gamma_h)\tilde{f}_{\gamma_g}(\gamma_g)$ can be obtained from the table of Mellin transforms provided in [40]. Based on (17), the exact PDF of the S-RIS-D link, $f_{\gamma_d}(\gamma_d)$, can be given by [14]

$$f_{\gamma_d}(\gamma_d) = \frac{\phi_d}{\gamma_d}\mathbf{G}_{2,6}^{6,0}\left[\frac{\psi_d\gamma_d}{\overline{\gamma}_d}\middle|\begin{matrix}\xi_h^2+1,\xi_g^2+1\\ \Delta_d\end{matrix}\right], \tag{18}$$

where $\phi_d = \phi_h\phi_g$, $\psi_d = \psi_h\psi_g$, $\overline{\gamma}_d = \overline{\gamma}_h\overline{\gamma}_g$, and $\Delta_d = \xi_g^2, \alpha_g, \beta_g, \xi_h^2, \alpha_h, \beta_h$. To obtain the corresponding CDF and MGF, we successively utilize Theorems 3 and 4 to (18), respectively exploiting [29, Eq. (07.34.21.0084.01)] and [31, Eq. (7.813.1)], and obtain [14]

$$F_{\gamma_d}(\gamma_d) = \phi_d\mathbf{G}_{3,7}^{6,1}\left[\frac{\psi_d\gamma_d}{\overline{\gamma}_d}\middle|\begin{matrix}1,\xi_h^2+1,\xi_g^2+1\\ \Delta_d,0\end{matrix}\right], \tag{19}$$

and

$$\Omega_{\gamma_d}(s) = \phi_d\mathbf{G}_{4,7}^{6,2}\left[\frac{\psi_d}{s\overline{\gamma}_d}\middle|\begin{matrix}0,1,\xi_h^2+1,\xi_g^2+1\\ \Delta_d,0\end{matrix}\right]. \tag{20}$$

3) $\gamma_o \leq \gamma_{th}$, S-D and S-RIS-D Links Combined Using the MRC Technique: In the MRC combining method, the combined SNR is given by (13). To obtain the PDF of the combined SNR, we apply Theorem 2 to change variables from γ_o and γ_d to γ_o^2 and γ_d^2, respectively. We redefine the combined SNR as $\gamma^{mrc} = \Gamma_o + \Gamma_d$, with Γ_o as γ_o^2 and Γ_d as γ_d^2. The PDF of γ^{mrc}, $f_{\gamma^{mrc}}(\gamma^{mrc})$ for $\gamma^{mrc} = \gamma_o^2 + \gamma_d^2$, is the convolution of the PDFs, $f_{\Gamma_o}(\Gamma_o)$ by $f_{\Gamma_d}(\Gamma_d)$ [40], [41], which can be evaluated using the Marichev's method, which is based on the Mellin convolution [14, Eq. (17)], [40], [41]. With the knowledge that SNRs are defined between 0 and $+\infty$, $f_{\Gamma_o}(\Gamma_o)$ and $f_{\Gamma_d}(\Gamma_d)$ can be found as follows: The expressions of $f_{\gamma_o}(\gamma_o)$ and $f_{\Gamma_d}(\Gamma_d)$ respectively given in (14) and (18), are valid for $0 \leq \gamma_o \leq +\infty$ and $0 \leq \gamma_d \leq +\infty$. Hence, let t: and u: $\mathbb{R} \Longrightarrow \mathbb{R}$ be two strictly continuous, monotonic, and differentiable functions, $\Gamma_o = \gamma_o^2 \Longrightarrow t(\gamma_o) = \gamma_o^2 \Longrightarrow t^{-1}(\Gamma_o) = \sqrt{\Gamma_o}$ and $\Gamma_d = \gamma_d^2 \Longrightarrow u(\gamma_d) = \gamma_d^2 \Longrightarrow u^{-1}(\Gamma_d) = \sqrt{\Gamma_d}$. We exploit Theorem 2 and obtain

$$f_{\Gamma_o}(\Gamma_o) = \frac{\phi_o}{2\Gamma_o}\mathbf{G}_{1,3}^{3,0}\left[\frac{\psi_o\sqrt{\Gamma_o}}{\overline{\gamma}_o}\middle|\begin{matrix}\xi_o^2+1\\ \xi_o^2,\alpha_o,\beta_o\end{matrix}\right] \tag{21}$$

and

$$f_{\Gamma_d}(\Gamma_d) = \frac{\phi_d}{2\Gamma_d}\mathbf{G}_{2,6}^{6,0}\left[\frac{\psi_d\sqrt{\Gamma_d}}{\overline{\gamma}_d}\middle|\begin{matrix}\xi_h^2+1,\xi_g^2+1\\ \xi_g^2,\alpha_g,\beta_g,\xi_h^2,\alpha_h,\beta_h\end{matrix}\right], \tag{22}$$

respectively. Next, we implement the Mellin convolution in the expressions in (21) and (22). With a change of variable of the type $A = \sqrt{B} \Longrightarrow B = A^2 \Longrightarrow dB = 2AdA$. Exploiting [29, Eq. (07.34.21.0011.01)], and a few mathematical operations, we obtain the PDF of the MRC combiner considering S-D and S-RIS-D links, $f_{\gamma^{mrc}}(\gamma^{mrc})$ as

$$f_{\gamma^{mrc}}(\gamma^{mrc}) = \frac{\phi_o\phi_d}{2\gamma}\mathbf{G}_{3,9}^{9,0}\left[\frac{\psi_o\psi_d\sqrt{\gamma}}{\overline{\gamma}_o\overline{\gamma}_d}\middle|\begin{matrix}\Phi_1\\ \Phi_2\end{matrix}\right], \tag{23}$$

where $\Phi_1 = \xi_o^2+1, \xi_h^2+1, \xi_g^2+1$ and $\Phi_2 = \xi_g^2, \alpha_g, \beta_g, \xi_h^2, \alpha_h, \beta_h, \xi_o^2, \alpha_o, \beta_o$. To obtain the corresponding CDF, $F_{\gamma^{mrc}}(\gamma^{mrc})$, we follow the steps in Theorem 3, which lead us to

$$F_{\gamma^{mrc}}(\gamma^{mrc}) = \frac{\phi_o\phi_d 2^{\varepsilon_m}}{16\pi^3}\mathbf{G}_{7,19}^{18,1}\left[\frac{\psi_o\psi_d\gamma}{2^{12}\overline{\gamma}_o\overline{\gamma}_d}\middle|\begin{matrix}1,\Delta_1\\ \Delta_2,0\end{matrix}\right], \tag{24}$$

where $\varepsilon_m = \alpha_g+\beta_g+\alpha_h+\beta_h+\alpha_o+\beta_o-5$, $\Delta_1 = (\xi_o^2+1)/2$, $(\xi_o^2+2)/2$, $(\xi_h^2+1)/2$, $(\xi_h^2+2)/2$, $(\xi_g^2+1)/2$, $(\xi_g^2+2)/2$, and $\Delta_2 = \xi_g^2/2$, $(\xi_g^2+1)/2$, $\alpha_g/2$, $(\alpha_g+1)/2$, $\beta_g/2$, $(\beta_g+1)/2$, $\xi_h^2/2$, $(\xi_h^2+1)/2$, $\alpha_h/2$, $(\alpha_h+1)/2$, $\beta_h/2$, $(\beta_h+1)/2$, $\xi_o^2/2$, $(\xi_o^2+1)/2$, $\alpha_o/2$, $(\alpha_o+1)/2$, $\beta_o/2$, $(\beta_o+1)/2$. Accordingly, we follow Theorem 4 to derive the corresponding MGF, $\Omega_{\gamma^{mrc}}(s)$, expressed as

$$\Omega_{\gamma^{mrc}}(s) = \frac{\phi_o\phi_d 2^{\varepsilon_m}}{16\pi^3}\mathbf{G}_{8,19}^{18,2}\left[\frac{\psi_o\psi_d}{2^{12}s\overline{\gamma}_o\overline{\gamma}_d}\middle|\begin{matrix}0,1,\Delta_1\\ \Delta_2,0\end{matrix}\right]. \tag{25}$$

IV. Performance Analysis

In this section, we examine both ergodic channel capacity and average BER for the three scenarios $\gamma_{th} \leq \gamma_o$, S-D link alone (LoS), $\gamma_o \leq \gamma_{th}$, S-RIS-D link alone (NLoS), and $\gamma_o \leq \gamma_{th}$, S-D and S-RIS-D links combined.

A. Analysis

1) $\gamma_{th} < \gamma_o$, S-D Link Alone (LoS): The PDF and CDF of the e2e SNR corresponding to this scenario, $f_{\gamma_o}(\gamma_o)$ and $F_{\gamma_o}(\gamma_o)$, respectively given in (14) and (15), are exploited to derive the channel capacity and average BER. We sequentially utilize Theorems 5 and 6 and obtain

$$\overline{C}_o = \frac{W\phi_o}{\log(2)} \mathbf{G}_{3,5}^{5,1}\left[\frac{2\pi\psi_o}{e\overline{\gamma}_o}\middle|\begin{matrix}0,1,\xi_o^2+1\\ \xi_o^2,\alpha_o,\beta_o,0,0\end{matrix}\right] \tag{26}$$

and

$$\overline{P}_o = \frac{\phi_o}{2\Gamma(p)} \mathbf{G}_{3,4}^{3,2}\left[\frac{\psi_o}{q\overline{\gamma}_o}\middle|\begin{matrix}1-p,1,\xi_o^2+1\\ \xi_o^2,\alpha_o,\beta_o,0\end{matrix}\right], \tag{27}$$

respectively.

2) $\gamma_o \leq \gamma_{th}$, S-RIS-D Link Alone (NLoS): In the case of a total interruption of the S-D link, the system relies solely on the NLoS path through the RIS module to connect the user. The SNR's PDF and CDF, $f_{\gamma_d}(\gamma_d)$ and $F_{\gamma_d}(\gamma_d)$ derived in (18) and (19), are exploited to find the ergodic channel capacity and average BER, respectively. We consecutively follow Theorems 5 and 6, which lead to

$$\overline{C}_d = \frac{W\phi_d}{\log(2)} \mathbf{G}_{4,8}^{8,1}\left[\frac{2\pi\psi_d}{e\overline{\gamma}_d}\middle|\begin{matrix}0,1,\xi_h^2+1,\xi_g^2+1\\ \Delta_d,0,0\end{matrix}\right] \tag{28}$$

and

$$\overline{P}_d = \frac{\phi_d}{2\Gamma(p)} \mathbf{G}_{4,7}^{6,2}\left[\frac{\psi_d}{q\overline{\gamma}_d}\middle|\begin{matrix}1-p,1,\xi_h^2+1,\xi_g^2+1\\ \Delta_d,0\end{matrix}\right]. \tag{29}$$

3) $\gamma_o \leq \gamma_{th}$, S-D and S-RIS-D Links Combined Using the MRC Technique: In this scenario, there is no total interruption of the S-D link; the system relies on both the LoS and NLoS paths to connect the user. The PDF and CDF of the e2e SNR, $f_{\gamma^{mrc}}(\gamma^{mrc})$ and $F_{\gamma^{mrc}}(\gamma^{mrc})$, given in (23) and (24), are used to find the ergodic channel capacity and average BER, respectively. We successively follow Theorems 5 and 6 and get

$$\overline{C}^{mrc} = \frac{W\phi_o\phi_d 2^{\varepsilon_m}}{16\pi^3\log(2)} \mathbf{G}_{8,20}^{20,1}\left[\frac{2\pi\left(\psi_o\psi_d\right)^2}{2^{12}e\left(\overline{\gamma}_o\overline{\gamma}_d\right)^2}\middle|\begin{matrix}0,1,\Delta_1\\ \Delta_2,0,0\end{matrix}\right] \tag{30}$$

and

$$\overline{P}^{mrc} = \frac{\phi_o\phi_d 2^{\varepsilon_b}}{32\pi^3\Gamma(p)} \mathbf{G}_{8,19}^{18,2}\left[\frac{\psi_o\psi_d}{2^{12}q\overline{\gamma}_o\overline{\gamma}_d}\middle|\begin{matrix}1-p,1,\Delta_1\\ \Delta_2,0\end{matrix}\right]. \tag{31}$$

B. Summary of the Analysis

Let γ_{e2e} be the e2e SNR of the entire system, including both S-D and S-RIS-D paths. The PDF, $f_{\gamma_{e2e}}(\gamma_{e2e})$, CDF, $F_{\gamma_{e2e}}(\gamma_{e2e})$, and MGF, $\Omega_{\gamma_{e2e}}(s)$, of γ_{e2e}, are respectively expressed with respect to the three defined scenarios (see Sections II and III, and Fig. 2). This is also the case for the ergodic channel capacity, $\overline{C}_{e2e}$, and average BER, $\overline{P}_{e2e}$. In Table II, the expressions for $f_{\gamma_{e2e}}(\gamma_{e2e}), F_{\gamma_{e2e}}(\gamma_{e2e}), \Omega_{\gamma_{e2e}}(s), \overline{C}_{e2e}$, and $\overline{P}_{e2e}$ for these three studied scenarios are summarized. Under normal conditions, there is no need to use the RIS module; the LoS link is enough to provide the required quality of service. $\gamma_{e2e} = \gamma_o$, $f_{\gamma_{e2e}}(\gamma_{e2e}) = f_{\gamma_o}(\gamma_o)$, $F_{\gamma_{e2e}}(\gamma_{e2e}) = F_{\gamma_o}(\gamma_o)$, $\overline{C}_{e2e} = \overline{C}_o$, and $\overline{P}_{e2e} = \overline{P}_o$. When $\gamma_o \leq \gamma_{th}$ with full LoS link interruption, the system relies on the S-RIS-D link alone to light the user, $\gamma_{e2e} = \gamma_d$, $f_{\gamma_{e2e}}(\gamma_{e2e}) = f_{\gamma_d}(\gamma_d), F_{\gamma_{e2e}}(\gamma_{e2e}) = F_{\gamma_d}(\gamma_d), \overline{C}_{e2e} = \overline{C}_d$, and $\overline{P}_{e2e} = \overline{P}_d$. Finally, when $\gamma_o \leq \gamma_{th}$ with a continuous degradation of the LoS link, the system exploits both the S-D and S-RIS-D links to connect the user, $\gamma = \gamma^{mrc}$, $f_{\gamma_{e2e}}(\gamma_{e2e}) = f_{\gamma^{mrc}}(\gamma^{mrc})$, $F_{\gamma_{e2e}}(\gamma_{e2e}) = F_{\gamma^{mrc}}(\gamma^{mrc})$, $\overline{C}_{e2e} = \overline{C}^{mrc}$, and $\overline{P}_{e2e} = \overline{P}^{mrc}$.

V. Numerical Results

A. Results

We consider an environment where the receiver is situated 1 km from the transmitter and follows the GG distribution. It is assumed that the receiver field-of-view is large enough to allow light from both the S-D and S-RIS-D links to reach the photodetector. The atmospheric turbulence, which is not the unique cause of signal degradation at D, is different between the two links, S-D and S-RIS-D, depending on whether or not the cloud is large enough to also cover the S-RIS-D link. The S-D link is characterized by the parameters obtained from [30], while the S-RIS-D link considers parameters from both [30] and [14], respectively. The transmission signal is characterized by a light of wavelength $\lambda = 785$ nm and wave number $\eta = 2\pi/\lambda$. The S-D link is affected by the refractive structure parameter $C_n^2 = 10^{-11}$ m$^{-2/3}$, 1.2×10^{-13} m$^{-2/3}$, and 2.8×10^{-13} m$^{-2/3}$, leading to atmospheric effects obtained from the Ritov variance ($\sigma_R^2 = 1.23 \times C_n^2 k_w^{7/6} L^{11/6}$) as $\alpha = 4.2, 2.296, 8$ and $\beta_o = 3, 2, 4$, respectively for the values of refractive structure enumerated above. The pointing error over the S-D link varies between 1 and 1.6. These values are used to evaluate the FSO link in [30]. The S-RIS-D link is characterized by the refractive structure parameter over the two sections S-RIS and RIS-D given by $C_n^2 = 2 \times 10^{-13}$ m$^{-2/3}$, which leads to values of atmospheric effects evaluated as $\alpha_h = 2.49$ and 4.92, $\alpha_g = 2.11$ and 4.2, $\beta_h = 3.90$ and 4.04, $\beta_g = 4.37$ and 3, respectively. The pointing error bears values 1, 1.1, 1.52, and 1.6. These values are practical values used to evaluate RIS-assisted FSO links in [14].

We evaluate the S-D and S-RIS-D links individually and both S-D and S-RIS-D links based on the MRC combining technique. We consider situations where $\gamma_{e2e} > \gamma_{th}$ (no need to use the OnD RIS module), $\gamma_{e2e} \leq \gamma_{th}$ and total interruption of the S-D link, where the user is illuminated through the OnD RIS module, and finally, $\gamma_{e2e} \leq \gamma_{th}$ with a continuous degradation of the S-D link. Here, the user is connected through both S-D and S-RIS-D links. We evaluate the average channel capacity, $\overline{C}_{e2e}$, and the average BER, $\overline{P}_{e2e}$, considering these three scenarios and several sets of values for the atmospheric effects and pointing errors. When the weather conditions over the S-D link

TABLE II
SUMMARY OF THE PROPOSED OND FSO SYSTEM

	$\gamma_o > \gamma_{th}$, S-D link alone	$\gamma_o \leq \gamma_{th}$, S-RIS-D link alone	$\gamma_o \leq \gamma_{th}$, S-D and S-RIS-D links combined
Channel Statistics			
$f_{\gamma_{e2e}}(\gamma_{e2e}) =$	$f_{\gamma_o}(\gamma_o)$	$f_{\gamma_d}(\gamma_d)$	$f_{\gamma^{mrc}}(\gamma^{mrc})$
$F_{\gamma_{e2e}}(\gamma_{e2e}) =$	$F_{\gamma_o}(\gamma_o)$	$F_{\gamma_d}(\gamma_d)$	$F_{\gamma^{mrc}}(\gamma^{mrc})$
$\Omega_{\gamma_{e2e}}(s) =$	$\Omega_{\gamma_o}(s)$	$\Omega_{\gamma_d}(s)$	$\Omega_{\gamma^{mrc}}(s)$
Performance Metrics			
$\overline{C}_{e2e} =$	$\overline{C}_o$	$\overline{C}_d$	$\overline{C}^{mrc}$
$\overline{P}_{e2e} =$	$\overline{P}_o$	$\overline{P}_d$	$\overline{P}^{mrc}$

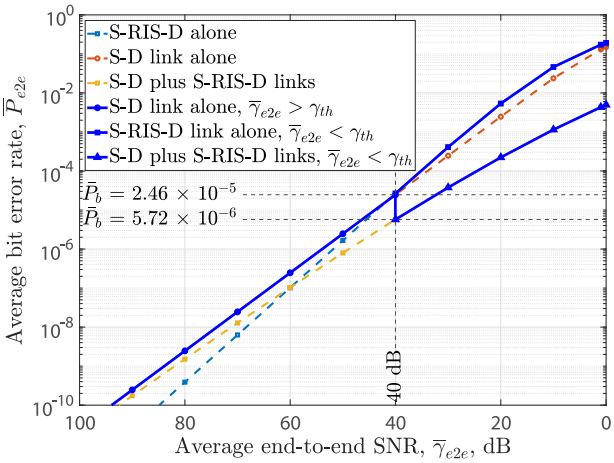

Fig. 3. Average BER of an OnD RIS-assisted FSO system: $(\alpha_o = 4.2, \beta_o = 3, \xi_o = 1)$, $(\alpha_h = 2.49, \beta_h = 3.90, \xi_h = 1.1)$, and $(\alpha_g = 2.11, \beta_g = 4.37, \xi_g = 1.52)$.

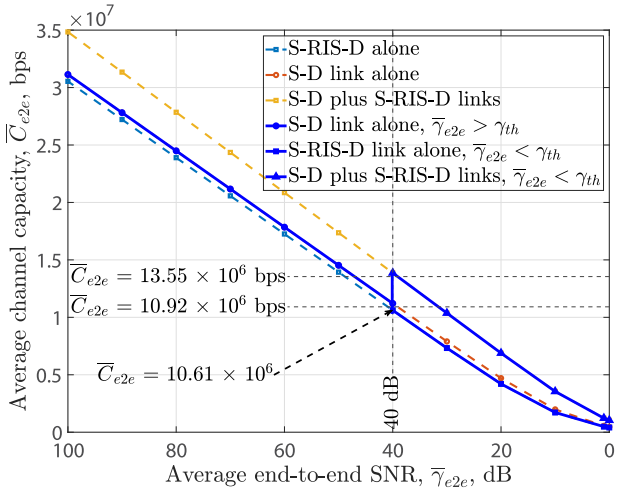

Fig. 4. Average ergodic channel capacity of an OnD RIS-assisted FSO system: $(\alpha_o = 4.2, \beta_o = 3, \xi_o = 1)$, $(\alpha_h = 2.49, \beta_h = 3.90, \xi_h = 1.1)$, and $(\alpha_g = 2.11, \beta_g = 4.37, \xi_g = 1.52)$.

worsen, the atmospheric effects, α_o and β_o drastically change. Consequently, the SNR decreases. If this condition persists, then the SNR continues to decrease until $\gamma_o = \gamma_{th}$. If the condition of the S-D link continuously worsens, γ_o drops below γ_{th}. As explained in Algorithm 1, this condition triggers the activation of the OnD RIS module. Part of the power generated by S reaches D through the OnD RIS module. The results of this evaluation are given in Figs. 3 to 8.

Figs. 3 and 4 depict $\overline{P}_{e2e}$ and $\overline{C}_{e2e}$ for $(\alpha_o = 4.2, \beta_o = 3, \xi_o = 1)$, $(\alpha_h = 2.49, \beta_h = 3.90, \xi_h = 1.1)$, and $(\alpha_g = 2.11, \beta_g = 4.37, \xi_g = 1.52)$, Figs. 5 and 6 depict $\overline{P}_{e2e}$ and $\overline{C}_{e2e}$ for $(\alpha_o = 2.29, \beta_o = 2, \xi_o = 1.6)$, $(\alpha_h = 2.49, \beta_h = 3.90, \xi_h = 1.1)$, and $(\alpha_g = 2.11, \beta_g = 4.37, \xi_g = 1.52)$, and Figs. 7 and 8 depict $\overline{P}_{e2e}$ and $\overline{C}_{e2e}$ for $(\alpha_o = 8, \beta_o = 4, \xi_o = 1)$, $(\alpha_h = 4.92, \beta_h = 4.04, \xi_h = 1)$, and $(\alpha_g = 4.2, \beta_g = 3, \xi_g = 1.6)$. In these evaluations, we consider the CBPSK scheme ($a = 0.5$ and $b = 1$). In all these figures, the horizontal axes are inverted to show the e2e SNR reduction (from 100 dB to 0 dB). The threshold e2e SNR, γ_{th}, is set to 40 dB. In all cases, the figures highlight the switch between links to improve the connection between S and D when the SNR drops below its threshold value. To ensure there is no signal interruption between S and D, when the e2e SNR drops below γ_{th}, the control unit enables the OnD RIS module so that it can contribute to connecting the user. This can be performed in two main situations: by using solely the S-RIS-D link or both links. This is materialized in all figures by the shift from the S-D link performance to that of either the S-RIS-D link or both the S-D and S-RIS-D links, depending on the situation.

In Fig. 3 $(\alpha_o = 4.2, \beta_o = 3, \xi_o = 1, \alpha_h = 2.49, \beta_h = 3.90, \xi_h = 1.1$, and $\alpha_g = 2.11, \beta_g = 4.37, \xi_g = 1.52)$, when the weather condition provokes the e2e SNR to drop below the threshold SNR, which corresponds to an average BER of 2.46×10^{-5}, the system switches to the S-RIS-D link at 2.46×10^{-5} average BER, and the system relies solely on the S-RIS-D path to connect the user. If the S-D link is not totally interrupted, the transmission switches from the S-D link to combined S-D and S-RIS-D links with an average BER of 5.72×10^{-6}. In Fig. 5 $(\alpha_o = 2.29, \beta_o = 2, \xi_o = 1.6, \alpha_h = 2.49, \beta_h = 3.90, \xi_h = 1.1$, and $\alpha_g = 2.11, \beta_g = 4.37, \xi_g = 1)$, the same pattern governs the transmission. When the e2e SNR drops below 40 dB, at a BER of 1.78×10^{-7}, the transmission shifts to the S-RIS-D link for a total interruption of the S-D path. The average BER at the switching point for the S-RIS-D link is 8.51×10^{-5}. However, if the S-D path can still transmit, then both links

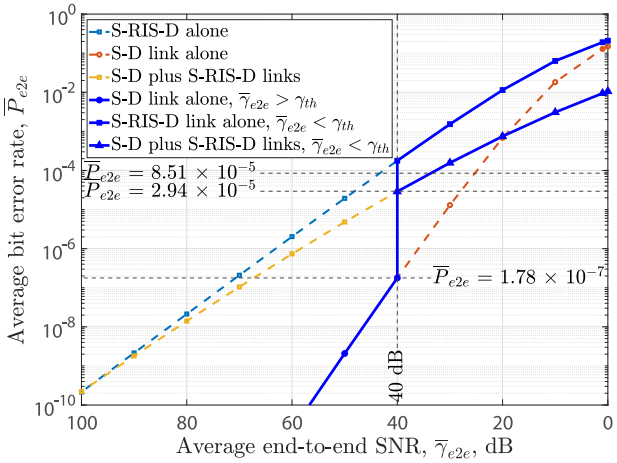

Fig. 5. Average BER of an OnD RIS-assisted FSO system: ($\alpha_o = 2.29, \beta_o = 2, \xi_o = 1.6$), ($\alpha_h = 2.49, \beta_h = 3.90, \xi_h = 1.1$), and ($\alpha_g = 2.11, \beta_g = 4.37, \xi_g = 1$).

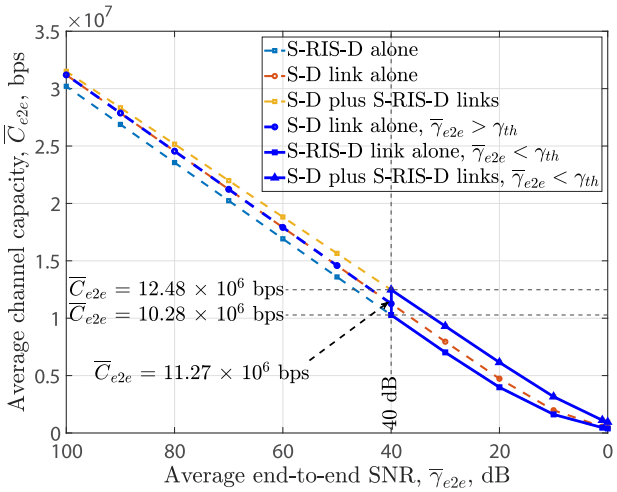

Fig. 6. Average ergodic channel capacity of an OnD RIS-assisted FSO system: ($\alpha_o = 2.29, \beta_o = 2, \xi_o = 1.6$), ($\alpha_h = 2.49, \beta_h = 3.90, \xi_h = 1.1$), and ($\alpha_g = 2.11, \beta_g = 4.37, \xi_g = 1$).

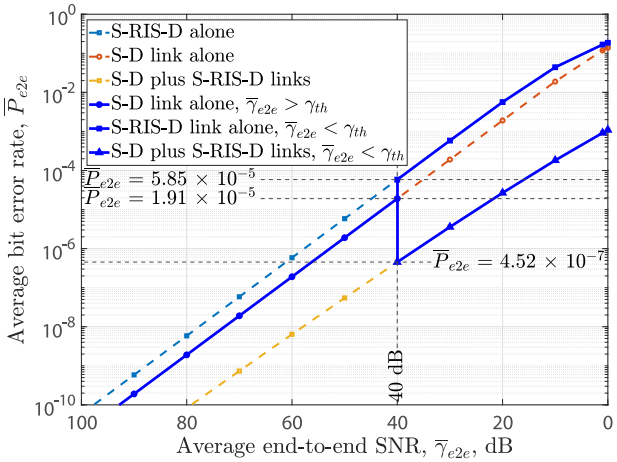

Fig. 7. Average BER of an OnD RIS-assisted FSO system: ($\alpha_o = 8, \beta_o = 4, \xi_o = 1$), ($\alpha_h = 4.92, \beta_h = 4.04, \xi_h = 1$), and ($\alpha_g = 4.2, \beta_g = 3, \xi_g = 1.6$).

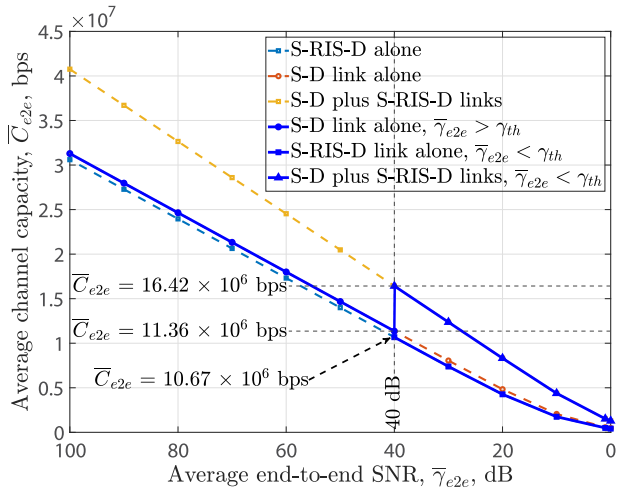

Fig. 8. Average ergodic channel capacity of an OnD RIS-assisted FSO system: ($\alpha_o = 8, \beta_o = 4, \xi_o = 1$), ($\alpha_h = 4.92, \beta_h = 4.04, \xi_h = 1$), and ($\alpha_g = 4.2, \beta_g = 3, \xi_g = 1.6$).

operate for an average BER of 2.94×10^{-5}. The same pattern is observed in Fig. 7 ($\alpha_o = 8, \beta_o = 4, \xi_o = 1, \alpha_h = 4.92, \beta_h = 4.04, \xi_h = 1$, and $\alpha_g = 4.2, \beta_g = 3, \xi_g = 1.6$), where switching happens at an average BER of 1.91×10^{-5}. When there is total interruption of the S-D path, the S-RIS-D link takes over with an average BER of 5.85×10^{-5}. With both links, when there is no total interruption of the S-D link, we obtain a switch to the combined S-D and S-RIS-D links with an average BER of 4.52×10^{-7}.

These results and switching scenarios can also be observed in Figs. 4, 6, and 8, where the e2e ergodic channel capacity switches between that of the S-D link and those of the S-RIS-D and both S-D and S-RIS-D links depending on the case. As shown in Fig. 4, for $\alpha_o = 4.2, \beta_o = 3, \xi_o = 1, \alpha_h = 2.49, \beta_h = 3.90, \xi_h = 1.1$, and $\alpha_g = 2.11, \beta_g = 4.37, \xi_g = 1.52$, the e2e capacity can switch from 10.92 Mbps (S-D link) to 10.61 Mbps (S-RIS-D link) for a total interruption or to 13.55 Mbps (S-D and S-RIS-D links) when the S-D link is degraded, but still transmits data. Figure 6 shows results for $\alpha_o = 2.29, \beta_o = 2, \xi_o = 1.6, \alpha_h = 2.49, \beta_h = 3.90, \xi_h = 1.1$, and $\alpha_g = 2.11, \beta_g = 4.37, \xi_g = 1$. The e2e capacity can switch from 11.27 Mbps (S-D link) to 10.28 Mbps (S-RIS-D link) for a total interruption or to 12.48 Mbps (S-D and S-RIS-D links) when the S-D is degraded and still transfers information. In Fig. 8 for $\alpha_o = 8, \beta_o = 4, \xi_o = 1$, $\alpha_h = 4.92, \beta_h = 4.04, \xi_h = 1$, and $\alpha_g = 4.2, \beta_g = 3, \xi_g = 1.6$, we obtain switching of the e2e ergodic channel capacity from 11.36 Mbps (S-D link) to 10.67 Mbps (S-RIS-D link) for a total interruption or to 16.42 Mbps (S-D and S-RIS-D links) when the S-D is degraded and still transfer information.

Figs. 3 to 8 illustrate the impact of OnD RIS technology on the e2e channel capacity and average BER of the system. Based on these numerical results, it can be concluded that the amount of energy required to manage the RIS module will be significantly reduced, and the excess energy can be exploited when the module is connected to the network. Regarding the duration of on and off times of the RIS module connection,

the proposed solution is developed for compensating the power consumption associated with multiplicative fading and the cost of pilot signals. In this way, the overall cost related to the RIS infrastructure will be substantially reduced.

B. Optimal Use of the OnD RIS Technology to Prevent FSO Link's Failure

To maintain higher transmission performance and quality-of-service, and comply with the requirements of 6G networks, it is imperative to ensure that the e2e SNR, or e2e channel capacity, does not fall below specific values. This implies that finding the system's parameters that optimize data transmission can be based on optimizing the e2e SNR, channel capacity, and/or minimizing the probability of error. If these values cannot remain constant, then the system should ensure that they are above a certain e2e channel capacity, e2e SNR, or below a certain probability of error. This will allow us to engage the OnD RIS infrastructure sooner and prevent the system from falling into an outage situation. This can be summarized as

$$\begin{cases} \gamma_{e2e} \geq \gamma_{\Delta} & (i) \\ \overline{C}_{e2e} \geq \overline{C}_{\Delta} & (ii) \\ \overline{P}_{e2e} \leq \overline{P}_{\Delta} & (iii) \end{cases}, \tag{32}$$

where γ_{Δ}, $\overline{C}_{\Delta}$, and $\overline{P}_{\Delta}$ are set to ensure outages are avoided. Meeting these conditions will allow the system to anticipate channel behaviors by enabling the OnD RIS module sooner or before the system falls, i.e., before the SNR degradation reaches γ_{th}. Equation (32)–(i) can be solved using a mixed integer programming method [42], [43]. On the other side, (32)–(ii) and (32)–(ii), which contain the Meijer-G function, are of the form

$$\mathbf{G}_{p,q}^{m,n}\left[Z\middle|\begin{matrix}\mathbf{a_p}\\ \mathbf{b}_q\end{matrix}\right] \geq y(Z), \tag{33}$$

which can be explored through the analysis of $\mathbf{G}_{p,q}^{m,n}\left[Z\middle|\begin{matrix}\mathbf{a_p}\\ \mathbf{b}_q\end{matrix}\right] = y(Z)$, satisfying the linear ordinary differential equation of the generalized hypergeometric type [44].

Figs. 9 and 10 depict the behavior of the ergodic channel capacity and average BER in an anticipated scenario of an OnD RIS-assisted FSO system for a set of selected turbulence and pointing error parameters. Both figures show that it is possible to anticipate the degradation of the transmission environment by enabling the OnD RIS earlier. In Fig. 9, when the average BER increases due to the degradation of the transmission environment, which is characterized by the decrease of the average SNR, anticipation occurs at $\gamma_{\Delta} = 60$ dB to switch the error probability from 1.9×10^{-7} to 6.40×10^{-9}, by inserting the RIS module into the channel. This is also observed in Fig. 10, where, for the same $\gamma_{\Delta} = 40$ dB, the average ergodic channel capacity switches from 18.00 Mbps to 24.54 Mbps by the insertion of the OnD RIS module. If the transmission conditions continue to worsen, it is seen that the average BER continues to increase and will reach the critical value of 1.91×10^{-5} at 20 dB instead of 40 dB. Similarly, the threshold ergodic channel capacity is reached at about 30 dB instead of 40 dB, which corresponds to the scenario where the S-D is solely considered.

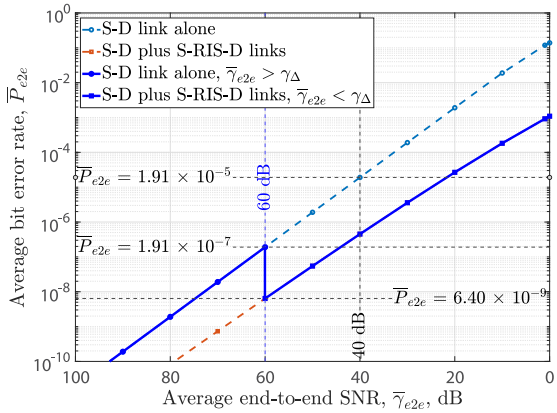

Fig. 9. Anticipated behavior of the average BER of an OnD RIS-assisted FSO system: $(\alpha_o = 8, \beta_o = 4, \xi_o = 1)$, $(\alpha_h = 4.92, \beta_h = 4.04, \xi_h = 1)$, and $(\alpha_g = 4.2, \beta_g = 3, \xi_g = 1.6)$.

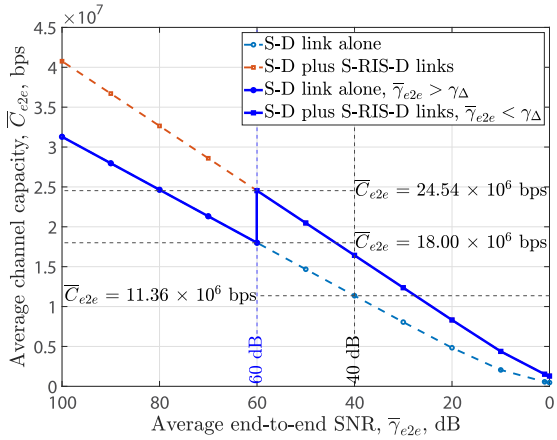

Fig. 10. Anticipated behavior of the ergodic channel capacity of an OnD RIS-assisted FSO system: $(\alpha_o = 8, \beta_o = 4, \xi_o = 1)$, $(\alpha_h = 4.92, \beta_h = 4.04, \xi_h = 1)$, and $(\alpha_g = 4.2, \beta_g = 3, \xi_g = 1.6)$.

C. Practical Considerations

The proposed OnD RIS module is composed of liquid crystals (LCs)-based elements with electronically controlled extinction coefficients. LCs possess the advantage of being well-known materials that can be easily deployed at a relatively low cost. It is important to note that the OnD RIS module is constructed from the same material throughout to ensure adequate hibernation when necessary. LC substance used has a coefficient of extinction greater than zero when the external field used to power the module is null. As a result, the module will not consume power while it is in hibernation mode.

VI. Future Research Directions and Conclusion

In this paper, we analyzed OnD RIS-assisted FSO systems for improved resource management. After defining the threshold and e2e SNR, we considered the scenario where the e2e SNR is greater than the threshold SNR. We also considered two

situations where the e2e SNR is lower than the threshold value. These two scenarios are respectively characterized by a total interruption of the S-D link and its degradation with substantial data transmission. For these three scenarios, we defined sub-channel SNRs. Afterward, we derived the e2e channel statistics, including the PDF, CDF, and MGF of the S-D link alone, the S-RIS-D link alone, and the combined S-D and S-RIS-D link based on the MRC combining technique. Exploiting these statistics, we derived, analyzed, and evaluated the e2e ergodic channel capacity and average BER, considering the CBPSK modulation scheme chosen as an example. We showed that in the FSO environment, the RIS module could be enabled just when needed. Moreover, we demonstrated through the MRC technique that when the S-D link is not totally disrupted, an optimal system performance can be recovered by introducing an RIS module into the environment. In addition, we showed that the RIS can be solicited in an OnD manner to prevent FSO link degradation when the weather conditions worsen.

The analysis presented in this paper is the first step of a pilot project on OnD RIS-assisted FSO systems, which provide several advantages, including resource and energy management. In accordance with the OnD RIS concept, it is essential to optimize the management of resources and energy in FSO systems. Recognizing that this is a requirement for the upcoming 6G, it is therefore important to use the RIS module precisely when needed. When the RIS module is not enabled, it hibernates. It will be inserted into the system exactly when the main transmission link is compromised. An optimization algorithm for such a system can be provided to prevent the channel from dropping below a threshold state or getting worse. This can be based on a mixed integer programming method [42], [43], or through the linear ordinary differential equation of the generalized hypergeometric function given that the Meijer-G function has generally been used in FSO systems analysis [44]. Such optimization can also reduce the use or solicitation of the RIS module. Overall, the system can be optimized to prevent degradation of the transmission environment from affecting data transmission. To do this, the RIS module can be introduced earlier into the system. This is an exciting research area that may be challenging and requires careful examination. The analysis and optimization of the OnD RIS phase shift, as well as its impact on the system's behavior and management of energy efficiency, is another critical aspect requiring careful attention. Furthermore, combining OnD RIS with artificial intelligence-based spectrum sensing, as discussed in [45] and [46], will maximize the benefits of both technologies in the 6G context. This area has the potential to be further investigated.

REFERENCES

[1] N. Chi et al., "Visible light communication in 6G: Advances, challenges, and prospects," *IEEE Veh. Technol. Mag.*, vol. 15, no. 4, pp. 93–102, Dec. 2020.

[2] A. R. Ndjiongue et al., "Maximal transmission rate in omni-DRIS-assisted indoor visible light communication systems," *IEEE Trans. Veh. Technol.*, vol. 73, no. 9, pp. 13956–13961, Sep. 2024.

[3] S. Aboagye et al., "Liquid crystal-based RIS for VLC transmitters: Performance analysis, challenges, and opportunities," *IEEE Wireless Commun.*, vol. 31, no. 4, pp. 98–105, Aug. 2024.

[4] B. Aly et al., "Vehicular VLC system with selection combining," *IEEE Trans. Veh. Technol.*, vol. 71, no. 11, pp. 12350–12355, Nov. 2022.

[5] P. Sharda et al., "Vehicular visible light communication system: Modeling and visualizing the critical outdoor propagation characteristics," *IEEE Trans. Veh. Technol.*, vol. 72, no. 11, pp. 14317–14329, Nov. 2023.

[6] J. Hong-Bae et al., "Free-space optical communications for 6G wireless networks: Challenges, opportunities, and prototype validation," *IEEE Commun. Mag.*, vol. 61, no. 4, pp. 116–121, Apr. 2023.

[7] A. Bekkali et al., "Free space optical communication systems for 6G: A modular transceiver design," *IEEE Wireless Commun.*, vol. 30, no. 5, pp. 50–57, Oct. 2023.

[8] C. H. de Souza et al., "Implementation of a hybrid FiWi system using FSO, VLC and mm-waves toward 6G applications," *IEEE Photon. Technol. Lett.*, vol. 35, no. 24, pp. 1403–1406, Dec. 2023.

[9] S. Aboagye et al., "RIS-assisted visible light communication systems: A tutorial," *IEEE Commun Surveys Tuts.*, vol. 25, no. 1, pp. 251–288, Firstquarter 2023.

[10] A. R. Ndjiongue et al., "Re-configurable intelligent surface-based VLC receivers using tunable liquid-crystals: The concept," *J. Lightw. Technol.*, vol. 39, no. 10, pp. 3193–3200, May 2021.

[11] A. R. Ndjiongue, T. M. N. Ngatched, O. A. Dobre, and H. Haas, "Design of a power amplifying-RIS for free-space optical communication systems," *IEEE Wireless Commun. Mag.*, vol. 28, no. 6, pp. 152–159, Dec. 2021.

[12] B. Xu et al., "Joint long-term energy efficiency optimization in C-RAN with hybrid energy supply," *IEEE Trans. Veh. Technol.*, vol. 69, no. 10, pp. 11128–11138, Oct. 2020.

[13] A. A. Ahmad et al., "Rate splitting multiple access in C-RAN: A scalable and robust design," *IEEE Trans. Commun.*, vol. 69, no. 9, pp. 5727–5743, Sep. 2021.

[14] A. R. Ndjiongue et al., "Analysis of RIS-based terrestrial-FSO link over G-g turbulence with distance and jitter ratios," *J. Lightw. Technol.*, vol. 39, no. 21, pp. 6746–6758, Nov. 2021.

[15] P. Agheli et al., "High-speed trains access connectivity through RIS-assisted FSO communications," *J. Lightw. Technol.*, vol. 40, no. 21, pp. 7084–7094, Nov. 2022.

[16] D. Wang et al., "Uplink secrecy performance of RIS-based RF/FSO three-dimension heterogeneous networks," *IEEE Trans. Wireless Commun.*, vol. 23, no. 3, pp. 1798–1809, Mar. 2024.

[17] M. Najafi et al., "Physics-based modeling and scalable optimization of large intelligent reflecting surfaces," *IEEE Trans. Commun.*, vol. 69, no. 4, pp. 2673–2691, Apr. 2021.

[18] M. Tayyab et al., "Signaling overhead and power consumption during handover in LTE," in *Proc. IEEE Wireless Commun. Netw. Conf.*, Marrakesh, Morocco, Apr. 2019, pp. 1–6.

[19] Z. Zhang et al., "Active RIS vs passive RIS: Which will prevail in 6G?," *IEEE Trans. Commun.*, vol. 71, no. 3, pp. 1707–1725, Mar. 2023.

[20] M. Najafi et al., "Intelligent reflecting surfaces for free space optical communication systems," *IEEE Trans. Commun.*, vol. 69, no. 9, pp. 6134–6151, Sep. 2021.

[21] H. Jia et al., "Ergodic capacity analysis for FSO communications with UAV-equipped IRS in the presence of pointing error," in *Proc. 20th IEEE Int. Conf. Commun. Technol.*, Nanning, China, Oct. 28–31, 2020, pp. 949–954.

[22] H. Ajam et al., "Channel modeling for IRS-assisted FSO systems," in *Proc. IEEE WCNC Conf.*, Nanjing, China, 2021, pp. 1–7.

[23] X. Pang et al., "IRS-assisted secure UAV transmission via joint trajectory and beamforming design," *IEEE Trans. Commun.*, vol. 70, no. 2, pp. 1140–1152, Feb. 2022.

[24] X. Pang, M. Sheng, N. Zhao, J. Tang, D. Niyato, and K.-K. Wong, "When UAV meets IRS: Expanding air-ground networks via passive reflection," *IEEE Wireless Commun. Mag.*, vol. 28, no. 5, pp. 164–170, Oct. 2021.

[25] Y. Su et al., "Spectrum and energy efficiency optimization in IRS-assisted UAV networks," *IEEE Trans. Commun.*, vol. 70, no. 10, pp. 6489–6502, Oct. 2022.

[26] A. R. Ndjiongue et al., "On-demand (OnD) RIS-assisted 6G networks: Concept, application, and future directions," Nov. 2023. [Online]. Available: http://dx.doi.org/10.36227/techrxiv.24471673.v1

[27] H. Pishro-Nik, *Introduction to Probability, Statistics, and Random Processes*. Blue Bell, PA, USA: Kappa Research, LLC, Aug. 2014.

[28] R. Maity, "Statistical methods in hydrology and hydroclimatology," in *Probability Distributions and Their Applications*. Berlin, Germany: Springer, 2022, pp. 91–140.

[29] "Mathematica edition-MeijerG, version 8," Wolfram Research, Inc., Champaign, IL, USA, Jan. 2010, pp. 1–163.

[30] I. Ansari et al., "Performance analysis of free-space optical links over málaga ($\mathcal{M}$) turbulence channels with pointing errors," *IEEE Trans. Wireless Commun.*, vol. 15, no. 1, pp. 91–102, Jan. 2016.
[31] I. M. Ryzhik and I. S. Gradshtein, *Table of Integrals, Series, and Products*, 8th ed. New York, NY, USA: Academic Press, Sep. 2014.
[32] L. Yang et al., "Accurate closed-form approximations to channel distributions of RIS-aided wireless systems," *IEEE Wireless Commun. Lett.*, vol. 9, no. 11, pp. 1985–1989, Nov. 2020.
[33] A. R. Ndjiongue et al., "On the capacity of RIS-assisted intensity-modulation optical channels," *IEEE Commun. Lett.*, vol. 26, no. 2, pp. 389–393, Feb. 2022.
[34] H. Xu et al., "RIS-assisted mmWave MIMO communications with finite-alphabet inputs and partial CSI," *IEEE Wireless Commun. Lett.*, vol. 13, no. 5, pp. 1339–1343, May 2024.
[35] Z. Chen et al., "Attention guided multi-task network for joint CFO and channel estimation in OFDM systems," *IEEE Trans. Wireless Commun.*, vol. 23, no. 1, pp. 321–333, Jan. 2024.
[36] T. Kim et al., "Semi-data-aided channel estimation for MIMO systems via reinforcement learning," *IEEE Trans. Wireless Commun.*, vol. 22, no. 7, pp. 4565–4579, Jul. 2023.
[37] X. Chen et al., "Adaptive statistical Bayesian MMSE channel estimation for visible light communication," *IEEE Trans. Signal Process.*, vol. 65, no. 5, pp. 1287–1299, Mar. 2017.
[38] F. Yilmaz et al., "A unified MGF-based capacity analysis of diversity combiners over generalized fading channels," *IEEE Trans. Commun.*, vol. 60, no. 3, pp. 862–875, Mar. 2012.
[39] A. P. Prodnikov et al., *Integral and Series Volume 3: More Special Functions*. London, U.K.: Gordon and Breach Science Publisher, Jan. 1986.
[40] "Mellin transform," Dec. 2003. Accessed: Dec. 10, 2023. [Online]. Available: https://en.wikipedia.org/wiki/Mellin_transform
[41] J. Bertrand et al., "The mellin transform," in *The Transforms and Applications Handbook*, 2nd ed. Boca Raton, FL, USA: CRC Press LLC, Feb. 2000, pp. 101–162.
[42] I. Kalesnikau et al., "Optimizing FSO networks resilient to adverse weather conditions by means of enhanced uncertainty sets," *Opt. Switching Netw.*, vol. 42, pp. 1–7, Nov. 2021.
[43] D. Nace et al., "An optimization model for robust FSO network dimensioning," *Opt. Switching Netw.*, vol. 32, pp. 25–40, Apr. 2019.
[44] A. Pishkoo et al., "Some applications of Meijer G-functions as solutions of differential equations in physical models," *J. Math. Phys., Anal., Geometry*, vol. 9, no. 3, pp. 379–391, Jan. 2013.
[45] B. Yang et al., "Intelligent spectrum learning for wireless networks with reconfigurable intelligent surfaces," *IEEE Trans. Veh. Technol.*, vol. 70, no. 4, pp. 3920–3925, Apr. 2021.
[46] B. Yang et al., "Spectrum-learning-aided reconfigurable intelligent surfaces for 'green' 6G networks," *IEEE Netw. Mag.*, vol. 35, no. 6, pp. 20–26, Nov./Dec. 2021.

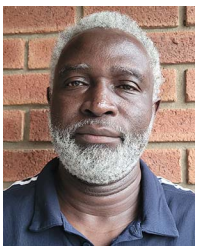

Alain R. Ndjiongue (Senior Member, IEEE) received the M.Eng. and D.Eng. degrees in electrical and electronic engineering from the University of Johannesburg, Johannesburg, South Africa, in 2013 and 2017, respectively. He was a Senior Lecturer with the University of Johannesburg, from 2017 to 2020. He was also a Senior Researcher with the Memorial University of Newfoundland, St. John's, NL, Canada. From 2022 to 2024, he was an Assistant Professor with the Memorial University of Newfoundland. Since September 2024, Dr. Ndjiongue has been an Associate Professor with the University of Witwatersrand, Johannesburg. His research interests include digital communications, including wireless, free space optical, visible light communications, and underwater optical communications. He also researches optical reconfigurable intelligent surfaces. Dr. Ndjiongue is an Associate Editor for IEEE COMMUNICATIONS LETTERS and IEEE OPEN JOURNAL OF THE COMMUNICATIONS SOCIETY. He is also an active Reviewer for several high-impact IEEE ComSoc journals and conferences. Dr. Ndjiongue was a 2017, 2018, and 2022 Exemplary Reviewer, and 2024 Exemplary Editor of IEEE COMMUNICATION LETTERS, Optical Society of America, and is a 2019 top 1% Peer Reviewer in Essential Science Indicators Research.

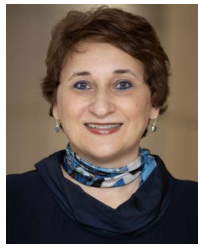

Octavia A. Dobre (Fellow, IEEE) is currently a Professor and Tier-1 Canada Research Chair with Memorial University, St. John's, NL, Canada. Her research interests include wireless communication and networking technologies, and optical and underwater communications. She has coauthored more than 500 refereed papers in these areas. Dr. Dobre is the VP Publications of the IEEE Communications Society. She was the inaugural Editor-in-Chief (EiC) of the IEEE OPEN JOURNAL OF THE COMMUNICATIONS SOCIETY and EiC of IEEE COMMUNICATIONS LETTERS. Dr. Dobre was a Fulbright Scholar, Royal Society Scholar, and Distinguished Lecturer of the IEEE Communications Society. She was the recipient of ten Best Paper Awards including the IEEE Heinrich Hertz Award. Dr. Dobre is an Elected Member of the European Academy of Sciences and Arts, Fellow of the Engineering Institute of Canada, Fellow of the Canadian Academy of Engineering, and Fellow of the Royal Society of Canada.

Hyundong Shin (Fellow, IEEE) received the B.S. degree in electronics engineering from Kyung Hee University (KHU), Yongin-si, South Korea, in 1999, and the M.S. and Ph.D. degrees in electrical engineering from Seoul National University, Seoul, South Korea, in 2001 and 2004, respectively. During his postdoctoral research with the Massachusetts Institute of Technology (MIT), Cambridge, MA, USA, from 2004 to 2006, he was with the Laboratory for Information Decision Systems (LIDS). In 2006, he joined the KHU, where he is currently a Professor with the Department of Electronic Engineering. His research interests include quantum information science, wireless communication, and machine intelligence. Dr. Shin was the recipient of the IEEE Communications Society's Guglielmo Marconi Prize Paper Award and William R. Bennett Prize Paper Award. He was the Publicity Co-Chair for the IEEE PIMRC, and Technical Program Co-Chair for the IEEE WCNC and IEEE GLOBECOM. He was an Editor of IEEE TRANSACTIONS ON WIRELESS COMMUNICATIONS and IEEE COMMUNICATIONS LETTERS.